Supporting Information for:

Investigation of the Diffusion of Cr_2O_3 into different phases of TiO_2 upon Annealing

Abdulrahman S. Alotabi [1,2,3], Christopher T. Gibson[1,3], Gregory F. Metha[4] and Gunther G. Andersson[1,3*]

[1] Flinders Institute for Nanoscale Science and Technology, Flinders University, Adelaide, South Australia 5042, Australia

[2] Department of Physics, Faculty of Science and Arts in Baljurashi, Albaha University, Baljurashi 65655, Saudi Arabia

[3] Flinders Microscopy and Microanalysis, College of Science and Engineering, Flinders University, 5042 Adelaide, Australia

[4] Department of Chemistry, University of Adelaide, Adelaide, South Australia 5005, Australia

*__Corresponding author:__ Gunther G. Andersson,

Email: gunther.andersson@flinders.edu.au.

Address: Physical Sciences Building (2111) GPO Box 2100, Adelaide 5001, South Australia

This supporting information document contains a detailed description about each of the applied characterisation techniques, and also presents the following additional figures and tables:

***Figure S1**: SEM cross-section image of the TiO_2 film deposited using the magnetron sputtering technique. The thickness of the TiO_2 film was determined to be 82 ± 5 nm.*

***Figure S2**: XRD patterns of Si wafer, $aTiO_2$, anatase, and anatase:rutile. The standard XRD patterns for anatase is PDF 01-075-1537 and rutile is PDF 01-071-4809.*

***Figure S3**: XRD pattern of anatase:rutile sample with Scherrer equation.*

***Figure S4:** Experimental procedure of photodeposition of the Cr_2O_3 layer.*

***Figure S5**: UPS spectra of (**A**) $aTiO_2$-Cr_2O_3, (**B**) anatase-Cr_2O_3, and (**C**) anatase:rutile-Cr_2O_3.*

***Figure S6**: XPS spectra of Cr 2p regions of (**A**) $aTiO_2$-Cr_2O_3, (**C**) anatase-Cr_2O_3, and (**E**) anatase:rutile-Cr_2O_3 and Ti 2p regions of (**B**) $aTiO_2$-Cr_2O_3, (**D**) anatase-Cr_2O_3, and (**F**) anatase:rutile-Cr_2O_3 as a function of annealing temperature.*

***Figure S7**: XPS spectra of O 1s regions of (**A**) $aTiO_2$-Cr_2O_3, (**C**) anatase-Cr_2O_3, and (**E**) anatase:rutile-Cr_2O_3 and C 1s regions of (**B**) $aTiO_2$-Cr_2O_3, (**D**) anatase-Cr_2O_3, and (**F**) anatase:rutile-Cr_2O_3 as a function of annealing temperature.*

***Figure S8**: AR-XPS spectra of (**A**) Cr 2p and (**B**) Ti 2p regions of $aTiO_2$-Cr_2O_3 at different angles.*

***Figure S9**: Concentration depth profiles deter of Cr and Ti of the Cr_2O_3 deposited onto the TiO_2 ($aTiO_2$-Cr_2O_3).*

***Figure S10**: XPS spectra of (**A**) Cr 2p of $aTiO_2$-Cr_2O_3, anatase-Cr_2O_3, and anatase:rutile-Cr_2O_3 before annealing.*

***Figure S11**: Cr 2p XP spectra of **(A)** $aTiO_2$ and **(B)** $aTiO_2$ after photodeposition of the Cr_2O_3 layer and calcining the sample at 200ºC for 10 min.*

***Figure S12**: XPS relative intensity of Ti 2p of $aTiO_2$-Cr_2O_3 and subsequently annealed to 600ºC. Then, the sample was sputtered for various times.*

***Figure S13**: Synchrotron XPS spectra of (**A**) Cr 2p and (**B**) Ti 2p regions of $aTiO_2$-Cr_2O_3 before and after annealing at 300℃ and 600℃. Fitted synchrotron XPS spectra of (**C and E**) Cr 2p and (**D and F**) Ti 2p of $aTiO_2$-Cr_2O_3 before and after annealing at 600℃.*

***Figure S14**: XRD patterns of Si wafer, $aTiO_2$-Cr_2O_3, anatase-Cr_2O_3, and anatase:rutile-Cr_2O_3 after annealing to 600℃. The standard XRD patterns for anatase is PDF 01-075-1537 and rutile is PDF 01-071-4809.*

***Figure S15**: UPS spectra of $aTiO_2$ and $aTiO_2$-Cr_2O_3 after annealing at various temperatures (**A**) 200℃, (**B**) 300℃, (**C**) 400℃, (**D**) 500℃ and (**E**) 600℃.*

***Figure S16**: AFM images of (**A**, **B** and **C**) $aTiO_2$ and (**D**, **E** and **F**) $aTiO_2$-Cr_2O_3. (The height scale for each image is the same and is 20 nm)*

***Table S1**: XPS peak positions of C 1s, O 1s, Cr $2p_{3/2}$ and Ti $2p_{3/2}$ of $aTiO_2$-Cr_2O_3, anatase-Cr_2O_3, and anatase:rutile-Cr_2O_3 samples as a function of annealing temperature.*

Methods:

- Scanning electron microscopy (SEM)

SEM measurement was performed to analyse the thickness of TiO_2 film using a FEI inspect F50 microscope. The SEM image was collected using an electron energy of 10 kV with a magnification of up to x120,000.

- Ultraviolet Photoelectron Spectroscopy (UPS)

UPS has been applied to determine the valance electron structure using Hel UV light with an excitation energy of 21.2 eV at a pass energy of 10 eV. The sensitivity of UPS can be up to a depth of 2-3 nm. The details of the method can be found elsewhere[1, 2].

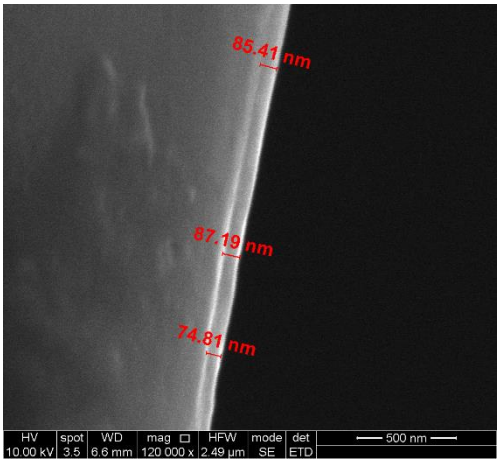

Figure S1*: SEM cross-section image of the TiO_2 film deposited using the magnetron sputtering technique. The thickness of the TiO_2 film was determined to be 82 ± 5 nm.*

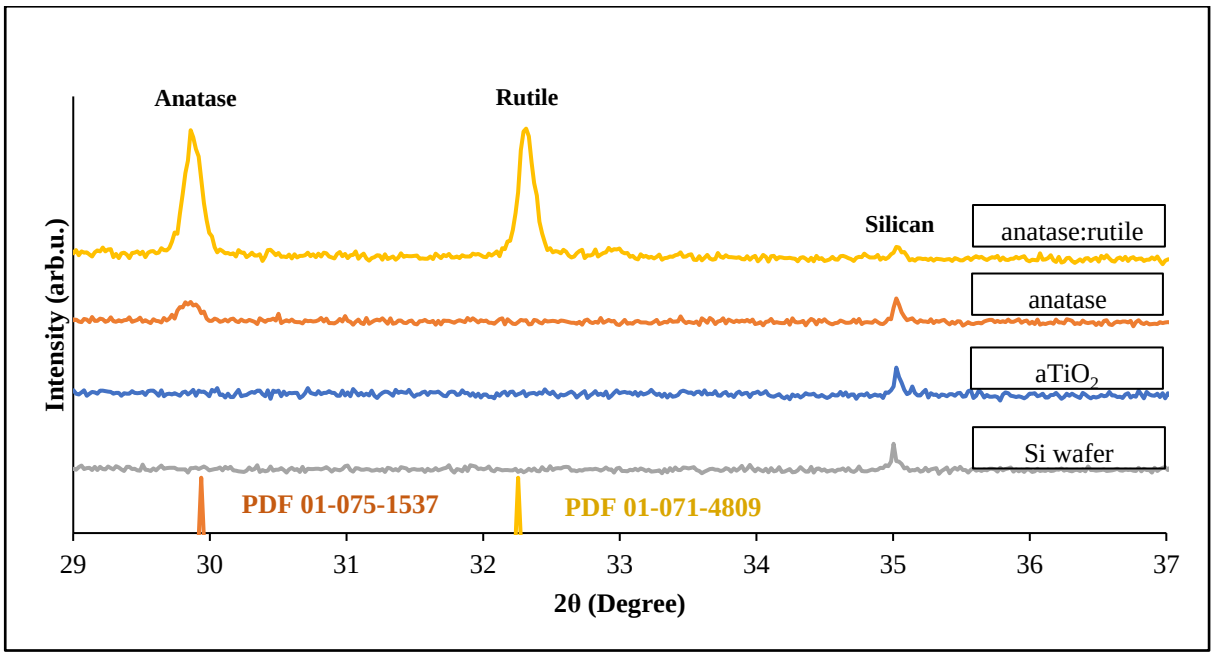

***Figure S2**: XRD patterns of Si wafer, $aTiO_2$, anatase, and anatase:rutile. The standard XRD patterns for anatase is PDF 01-075-1537, and rutile is PDF 01-071-4809.*

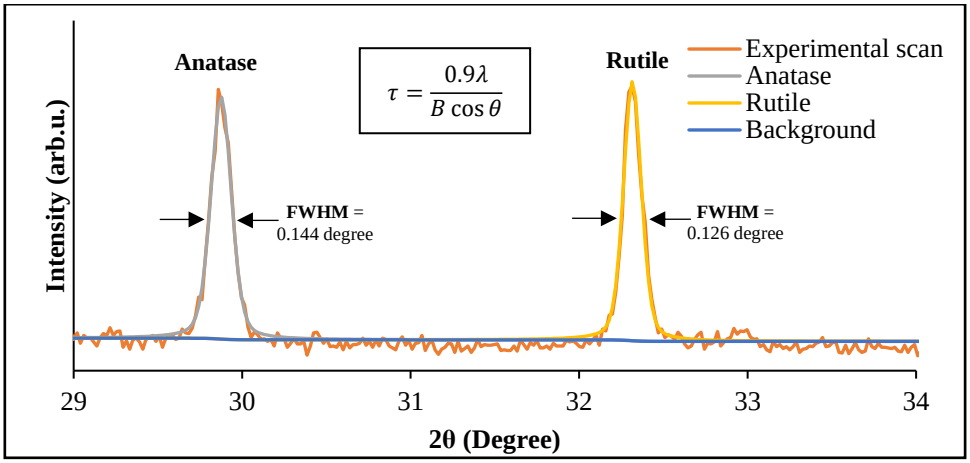

***Figure S3**: XRD pattern of anatase:rutile sample with Scherrer equation.*

Crystalline domain size can be calculated using the Scherrer equation. Figure S3 shows XRD pattern of anatase:rutile sample with the Scherrer equation $\tau = \frac{0.9\lambda}{B\cos\theta}$: where τ is the average crystalline domain size in Å, λ the wavelength of the X-ray source, B the full width at half maximum(FWHM) and θ the diffraction angle. The average crystalline domain size of anatase in anatase:rutile sample is: $\tau = \frac{0.9x0.179}{0.144\cos 29.88} = 66.3$ Å $= 6.63 \pm 0.1$ nm. The average crystalline domain size of rutile in anatase:rutile sample is: $\tau = \frac{0.9x0.179}{0.126\cos 32.32} = 76.2$ Å $= 7.62 \pm 0.1$ nm.

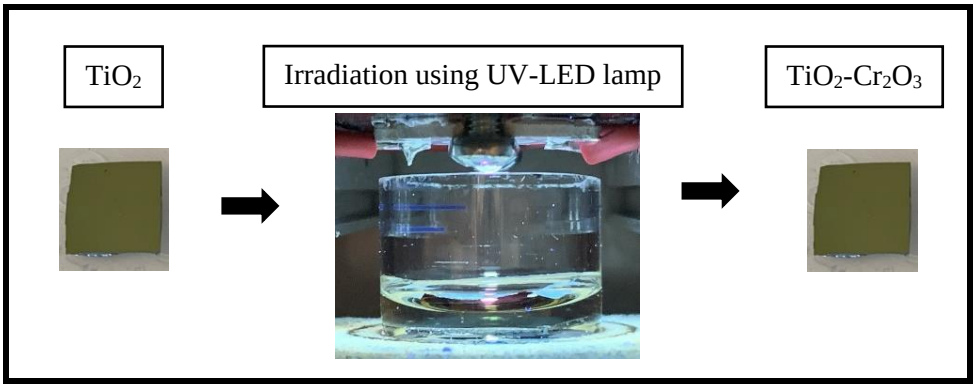

Figure S4: *Experimental procedure of photodeposition of the Cr_2O_3 layer.*

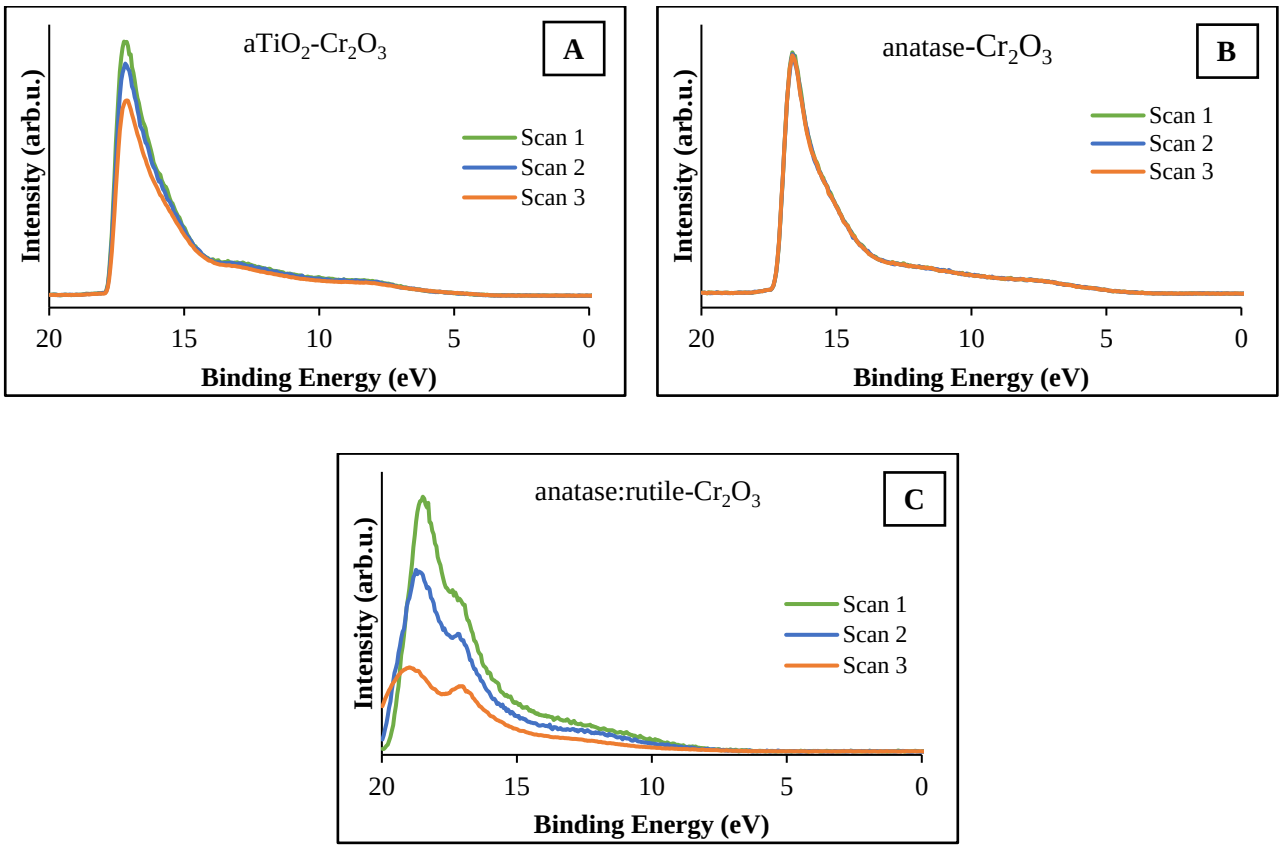

Figure S5*: UPS spectra of (**A**) $aTiO_2$-Cr_2O_3, (**B**) anatase-Cr_2O_3, and (**C**) anatase:rutile-Cr_2O_3.*

The binding energies of the XP spectra of the $aTiO_2$-Cr_2O_3 and the anatase-Cr_2O_3 samples were used as measured and not calibrated by setting the main C 1s peak to 285 eV. The binding energies are shown in Table 1S. The reason is twofold. Firstly, it can be seen from the UP spectra shown in Figure S5 that both samples are not subject to charging while acquiring UP spectra. In Figure S5A and S5B,

three consecutive spectra of both samples are shown. The shape of the three immediately consecutive spectra is identical and the secondary electron cut-off does not shift. Secondly, the position of O 1s and Ti $2p_{3/2}$ is the same within experimental uncertainty as well as the C 1s for the samples heated to 200°C and higher temperatures. Note that the C 1s peak for the non-heated sample is found at 285.4 eV. We assume that the C 1s peak of the non-heated sample stems from slightly oxidized hydrocarbons found on the sample, which could be due to solvent molecules remaining on the sample surface following cleaning of the sample, or photo-oxidation of hydrocarbons on the titania surface. If the energy scale of these two samples were calibrated by setting the main C 1s peak to 285 eV, the binding energies of O and Ti would move upon heating. Such a change in O and Ti binding energies upon mild heating cannot be rationalized by a chemical process. Based on this procedure, the binding energy of Ti is found at 459.2 ± 0.2 eV and can be assigned to Ti in TiO_2[3]. The binding energy of O is found at 530.5 ± 0.2 eV and can be assigned to O in TiO_2, which is the same binding energy of O in Cr_2O_3[3, 4]. A second and smaller O 1s peak is found for the non-heated sample at 532.2 eV, which could be related to H_2O or OH^- from the Cr deposition process. The binding energy of C for the non-heated sample is found at 285.4 ± 0.2 eV and is assumed to represent slightly oxidized C. The binding energy of C after annealing to 200°C and higher temperatures is found at 284.8 ± 0.2 eV and can be assigned to C in C-C bonds[5, 6]. The binding energy of Cr of the non-heated sample is found at 577.9 ± 0.2 eV eV and can be assigned to Cr_2O_3 or could also be $Cr(OH)_3$[7, 8]. The binding energy of Cr after annealing to 200°C and higher temperatures, is found at 577.1 ± 0.2 eV and can be assigned to Cr_2O_3[7, 8].

In contrast, the anatase:rutile-Cr_2O_3 sample did show charging and the above procedure cannot be applied to this sample. As can be seen in Figure S5C, the UP spectra of this sample shows a change in shape of the spectra and a shift to the left on the binding energy scale from scan 1 to 3. From this observation, it can be concluded that the sample is charging during electron spectroscopy. This could be due to various reasons like mounting of the sample on the sample holder or poor electrical contact between the TiO_2 layer and the Si substrate. For this sample we have calibrated the XP spectra by

setting the O 1s peak to the average of the binding energy of the O 1s peak in the $aTiO_2$-Cr_2O_3 and anatase-Cr_2O_3 samples. With this calibration, the binding energy of Ti $2p_{3/2}$ is found at 459.2 ± 0.2 eV, which is the same as for the $aTiO_2$-Cr_2O_3 and the anatase-Cr_2O_3 samples. The Cr $2p_{3/2}$ is found for the heated samples at 577.4 ± 0.2 eV, which is within error the same as for the $aTiO_2$-Cr_2O_3 and the anatase-Cr_2O_3 samples. The binding energy of Cr of the non-heated sample is somewhat higher and could also indicate the presence of $Cr(OH)_3$. The C 1s peak is found for the non-heated sample at 285.6 ± 0.2 eV, and for the heated sample at 284.8 ± 0.2 eV, which is the same as for the $aTiO_2$-Cr_2O_3 and the anatase-Cr_2O_3 samples. The C species of this sample are thus assigned to the same compounds as for the $aTiO_2$-Cr_2O_3 and the anatase-Cr_2O_3 samples.

Table S1*: XPS peak positions of C 1s, O 1s, Cr $2p_{3/2}$ and Ti $2p_{3/2}$ of $aTiO_2$-Cr_2O_3, anatase-Cr_2O_3, and anatase:rutile-Cr_2O_3 samples as a function of annealing temperature. For C and O, the position of the main peak is shown.*

Sample \ Element		Peak position (eV)			
		C 1s	O 1s	Ti $2p_{3/2}$	Cr $2p_{3/2}$
$aTiO_2$-Cr_2O_3	Non-heated	285.4 ± 0.2	530.4 ± 0.2	459.0 ± 0.2	577.9 ± 0.2
	200°C	284.9 ± 0.2	530.6 ± 0.2	459.2 ± 0.2	577.1 ± 0.2
	300°C	284.7 ± 0.2	530.6 ± 0.2	459.2 ± 0.2	577.2 ± 0.2
	400°C	284.7 ± 0.2	530.5 ± 0.2	459.2 ± 0.2	577.2 ± 0.2
	500°C	284.7 ± 0.2	530.6 ± 0.2	459.2 ± 0.2	577.1 ± 0.2
	600°C	284.8 ± 0.2	530.7 ± 0.2	459.3 ± 0.2	----
anatase-Cr_2O_3	Non-heated	285.4 ± 0.2	530.6 ± 0.2	459.4 ± 0.2	578.1 ± 0.2
	200°C	284.8 ± 0.2	530.5 ± 0.2	459.2 ± 0.2	576.9 ± 0.2
	300°C	284.5 ± 0.2	530.4 ± 0.2	459.1 ± 0.2	577.1 ± 0.2
	400°C	284.5 ± 0.2	530.3 ± 0.2	459.1 ± 0.2	577.0 ± 0.2
	500°C	284.4 ± 0.2	530.3 ± 0.2	459.1 ± 0.2	577.2 ± 0.2
	600°C	285.4 ± 0.2	530.4 ± 0.2	459.1 ± 0.2	----
anatase:rutile-Cr_2O_3	Non-heated	285.6 ± 0.2	530.5 ± 0.2	459.3 ± 0.2	578.1 ± 0.2
	200°C	285.3 ± 0.2	530.5 ± 0.2	459.2 ± 0.2	577.4 ± 0.2
	300°C	285.0 ± 0.2	530.5 ± 0.2	459.2 ± 0.2	577.3 ± 0.2
	400°C	284.8 ± 0.2	530.5 ± 0.2	459.2 ± 0.2	577.5 ± 0.2
	500°C	284.9 ± 0.2	530.5 ± 0.2	459.3 ± 0.2	577.7 ± 0.2
	600°C	285.1 ± 0.2	530.5 ± 0.2	459.1 ± 0.2	577.5 ± 0.2

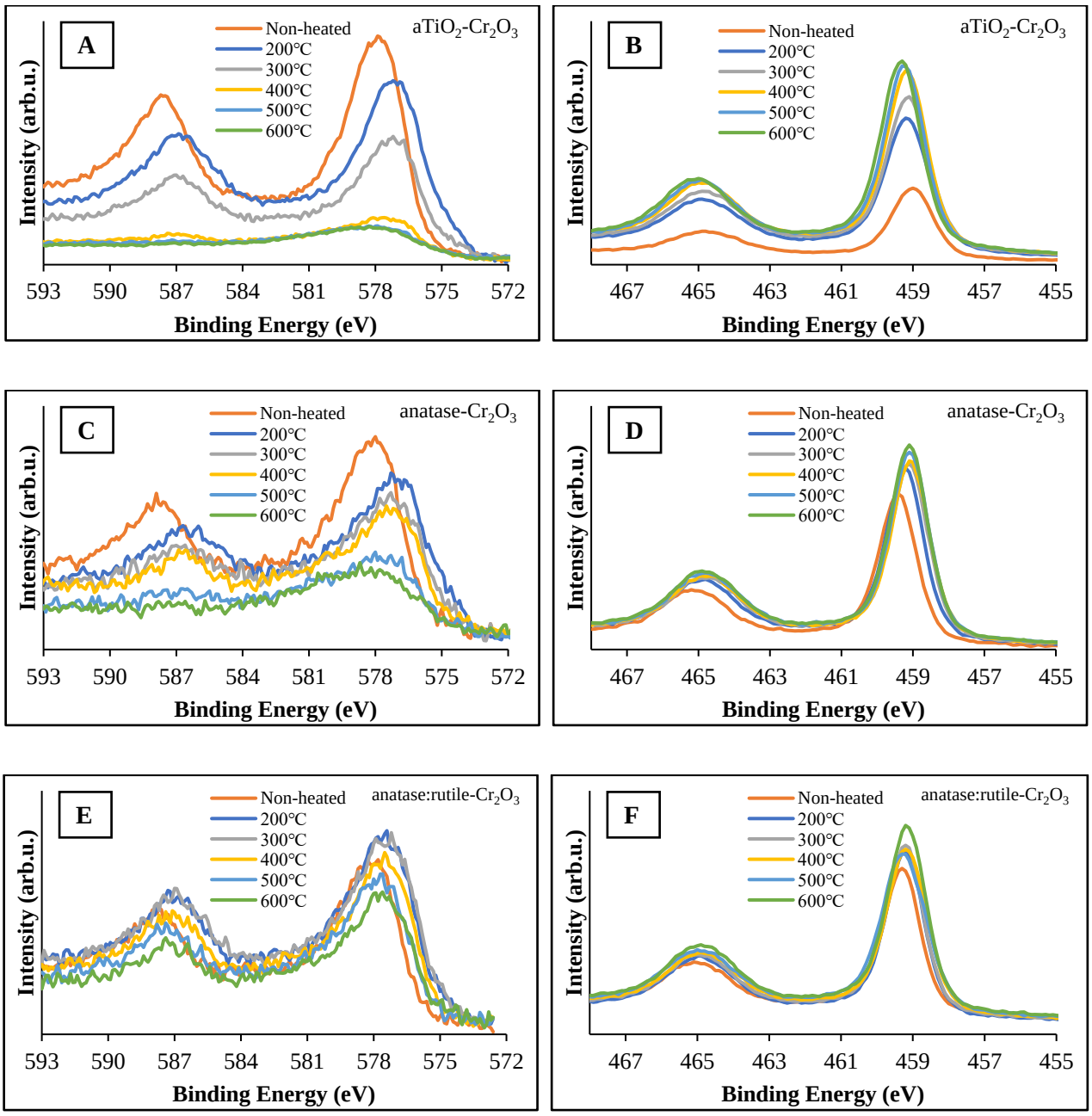

***Figure S6**: XPS spectra of Cr 2p regions of (**A**) aTiO2-Cr2O3, (**C**) anatase-Cr2O3, and (**E**) anatase:rutile-Cr2O3 and Ti 2p regions of (**B**) aTiO2-Cr2O3, (**D**) anatase-Cr2O3, and (**F**) anatase:rutile-Cr2O3 as a function of annealing temperature.*

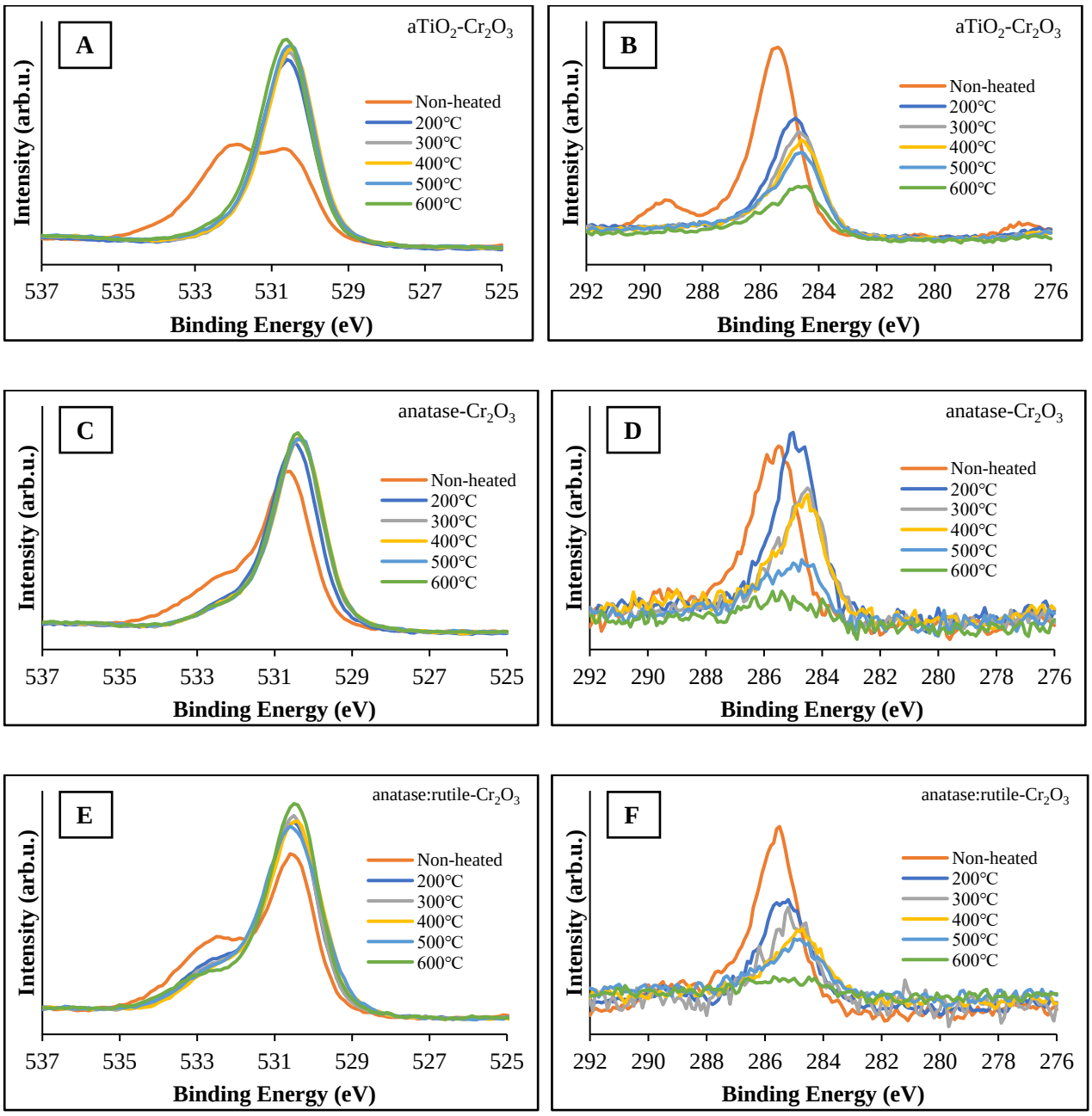

***Figure S7**: XPS spectra of O 1s regions of (**A**) aTiO2-Cr2O3, (**C**) anatase-Cr2O3, and (**E**) anatase:rutile-Cr2O3 and C 1s regions of (**B**) aTiO2-Cr2O3, (**D**) anatase-Cr2O3, and (**F**) anatase:rutile-Cr2O3 as a function of annealing temperature.*

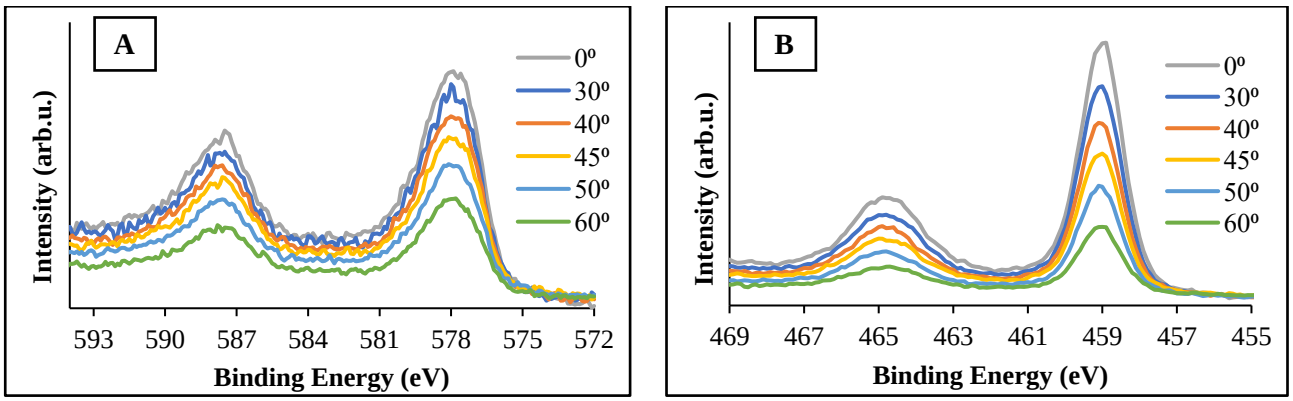

***Figure S8**: AR-XPS spectra of (**A**) Cr 2p and (**B**) Ti 2p regions of aTiO₂-Cr₂O₃ at different angles.*

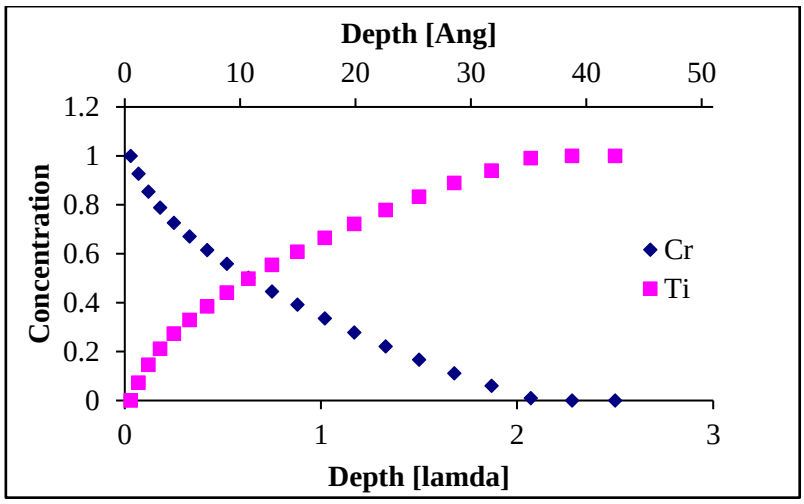

***Figure S9**: Concentration depth profiles deter of Cr and Ti of the Cr_2O_3 deposited onto the TiO_2 ($aTiO_2$-Cr_2O_3).*

The concentration depth profile of Cr and Ti of a TiO_2-Cr_2O_3 sample determined using AR-XPS is shown in Figure S9. We have applied the procedure described in detail by Eschen et al [9] using a single excitation energy [10] to determine the thickness of Cr layer. The depth profile for $aTiO_2$-Cr_2O_3 interpreted that Cr has a thickness of ~ 11 Å (1.1 nm). The usual crystal structure of Cr2O3 is corundum. 11 Å correspond to approximately two unit cells of Cr2O3. We have no evidence which crustal structure Cr2O3 forms in the present experiments.

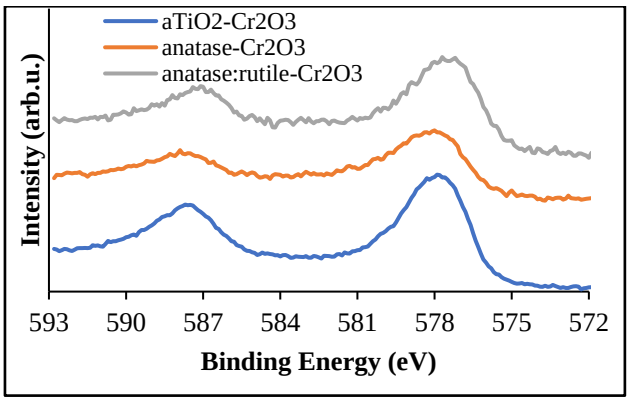

***Figure S10**: XPS spectra of (**A**) Cr 2p of $aTiO_2$-Cr_2O_3, anatase-Cr_2O_3, and anatase:rutile-Cr_2O_3 before annealing.*

Figure S10 shows the Cr 2p spectra of $aTiO_2$-Cr_2O_3, anatase-Cr_2O_3, and anatase:rutile-Cr_2O_3. The binding energy of Cr $2p_{3/2}$ appear at 577.8 ± 0.2 eV for Cr photodeposited onto various substrates, which corresponding to Cr_2O_3.

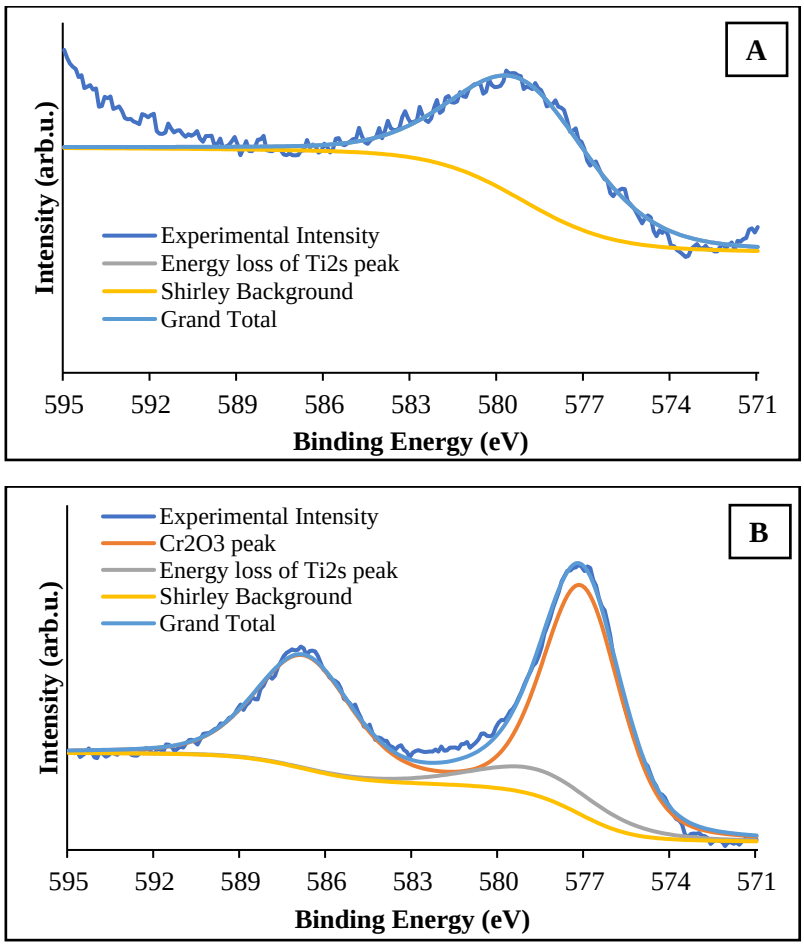

***Figure S11**: Cr 2p XP spectra of **(A)** $aTiO_2$ and **(B)** $aTiO_2$ after photodeposition of the Cr_2O_3 layer and calcining the sample at 200ºC for 10 min.*

Figure S11A shows the spectrum in the Cr 2p region for the aTiO_2 sample. It shows a peak with broad FWHM, which is the energy loss peak of the Ti 2s peak. This peak was also observed by Trenczek-Zajac [11]. Figure S11B shows the Cr 2p spectrum after the photodeposition of a chromium oxide layer and heating at ultrahigh vacuum conditions for 10 min at 200ºC. The position of the Cr $2p_{3/2}$ peak at 577.2 ± 0.2 eV allows for identifying this peak as Cr_2O_3 [8].

The energy loss peak of the Ti 2s peak overlaps with the Cr $2p_{3/2}$ peak at ~578.8 eV. The binding energy of this energy loss peak was calibrated according to Ti $2p_{3/2}$ (~459.4 eV) with the addition of 119.4 eV, and the FWHM was fixed at 5.4 eV. The area of the energy loss peak was identified by dividing the fitted area of Ti $2p_{3/2}$ on a relative factor of 8.35. Estimation of the Ti 2s energy loss peak was essential to correctly determine the chemical state of Cr.

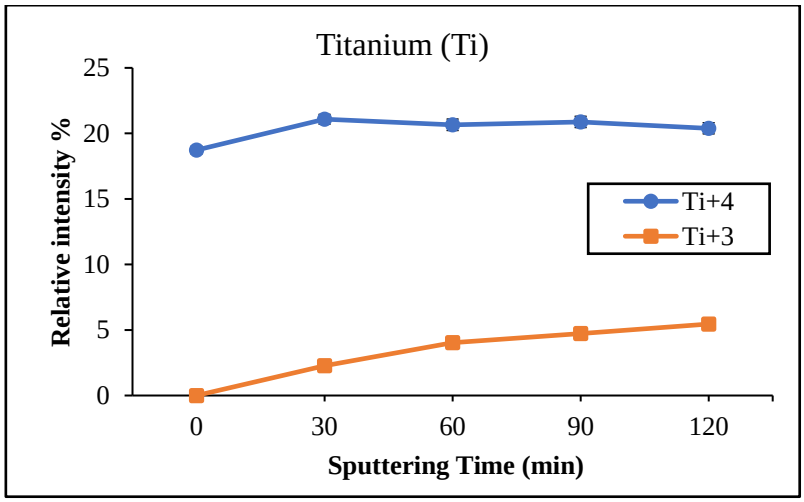

***Figure S12**: XPS relative intensity of Ti 2p of aTiO_2-Cr_2O_3 and subsequently annealed to 600ºC. Then, the sample was sputtered for various times.*

Figure S12 shows the relative intensity of TiO_2 peaks at different sputtering dose for both Ti^{4+} and Ti^{3+}. When the TiO_2 is sputtered, a second Ti $2p_{3/2}$ doublet was found at 457.6 ± 0.2 eV that corresponds to Ti^{3+} and the presence of O vacancies due to the sputtering [12]. In Figure S9, it can be seen that Ti^{4+} decreased slightly and Ti^{3+} increased with increasing sputter dose.

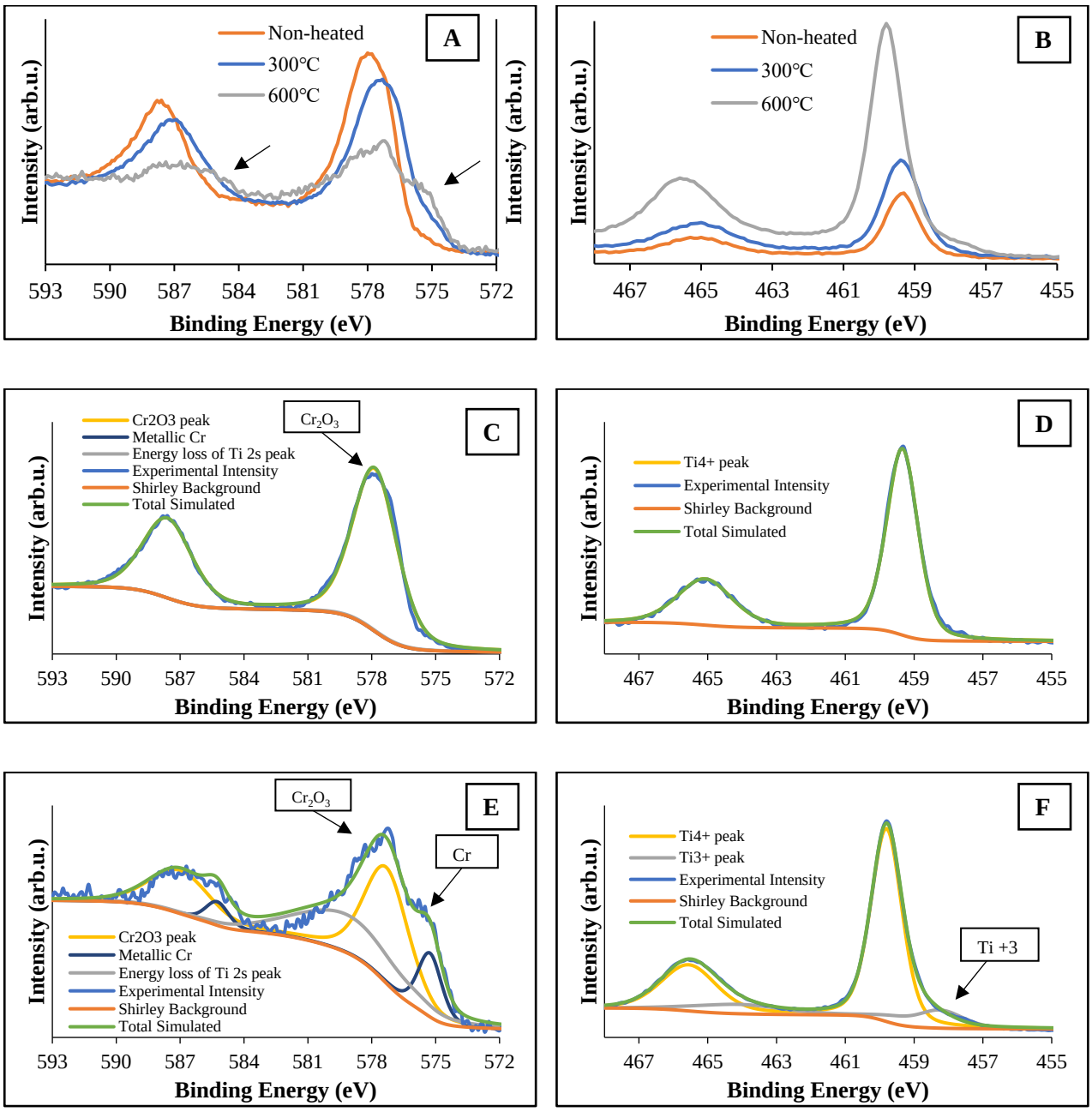

***Figure S13**: Synchrotron XPS spectra of (**A**) Cr 2p and (**B**) Ti 2p regions of aTiO₂-Cr₂O₃ before and after annealing at 300℃ and 600℃. Fitted synchrotron XPS spectra of (**C and E**) Cr 2p and (**D and F**) Ti 2p of aTiO₂-Cr₂O₃ before and after annealing at 600℃. A small amount of Ti^{3+} is formed when heating the samples to 600℃.*

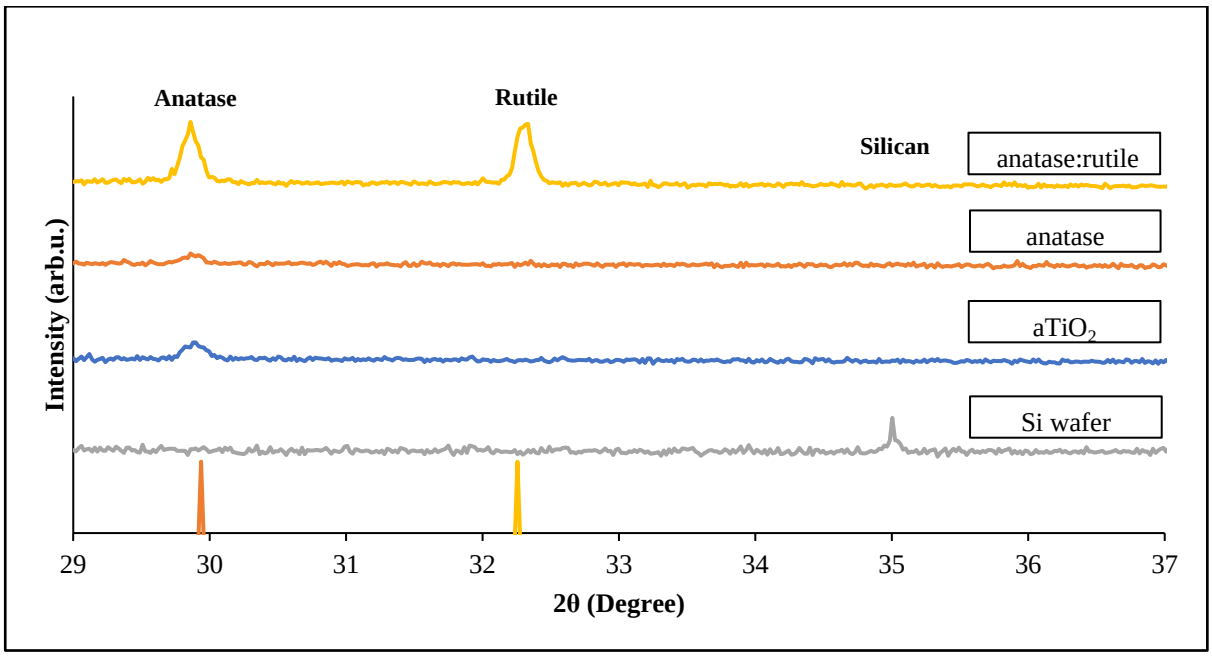

***Figure S14**: XRD patterns of Si wafer, aTiO₂-Cr₂O₃, anatase-Cr₂O₃, and anatase:rutile-Cr₂O₃ after annealing to 600℃. The standard XRD patterns for anatase is PDF 01-075-1537 and rutile is PDF 01-071-4809.*

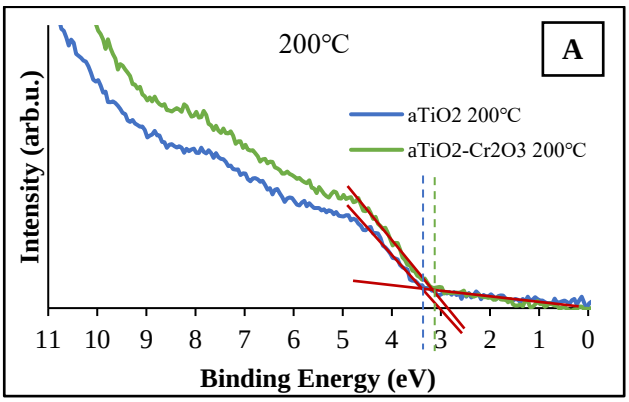

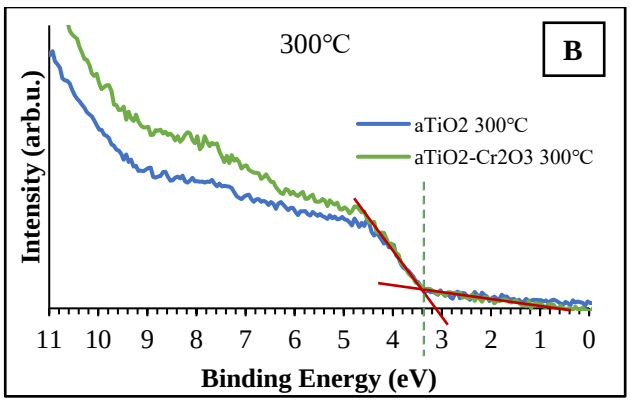

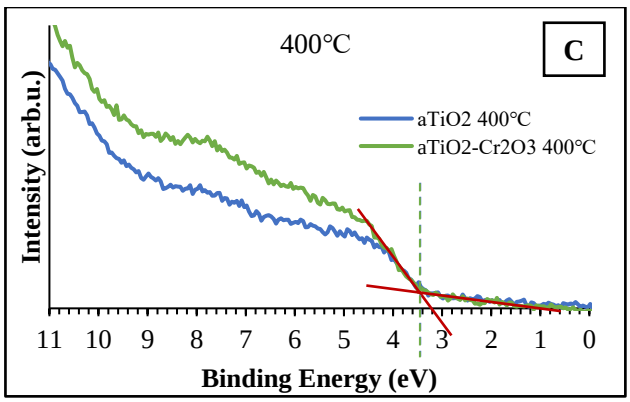

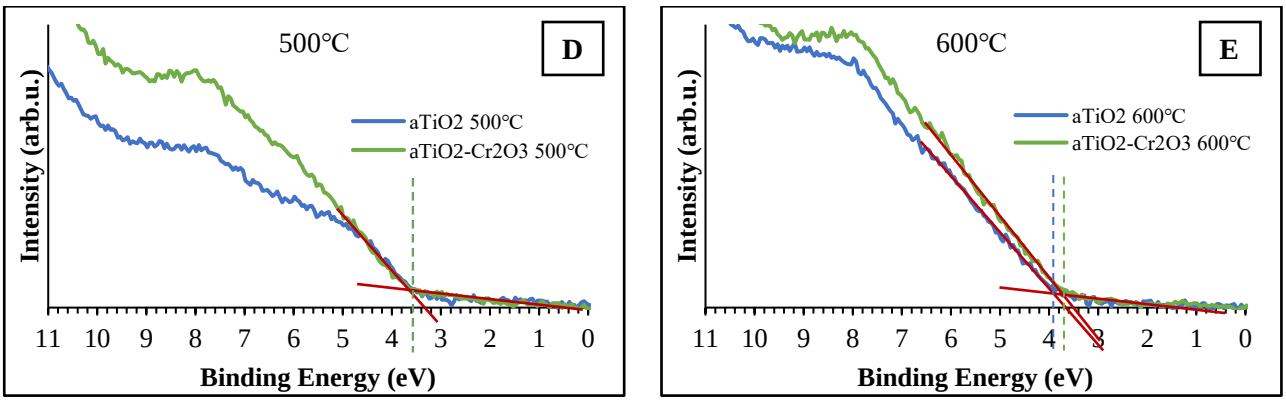

***Figure S15**: UPS spectra of $aTiO_2$ and $aTiO_2$-Cr_2O_3 after annealing at various temperatures (**A**) 200°C, (**B**) 300°C, (**C**) 400°C, (**D**) 500°C and (**E**) 600°C.*

Figure S15 shows the valence electron spectra (UPS) of $aTiO_2$ and $aTiO_2$-Cr_2O_3 as function of annealing temperatures. The edge of the valences band is indicated in the figures with a dash line (the blue dash line is $aTiO_2$ and green dash line is $aTiO_2$-Cr_2O_3). After annealing at 200°C, the valance band is found for $aTiO_2$ and $aTiO_2$-Cr_2O_3 at ~ 3.1 eV and ~ 3.4 eV, respectively. Annealing to 300°C up to 500°C shows same valance band for both samples around ~ 3.4 eV. The valance band shifted to higher binding energy after annealing at 600°C to ~ 3.9 eV and ~ 3.7 eV for $aTiO_2$ and $aTiO_2$-Cr_2O_3. UPS valance band structure measurements of $aTiO_2$ and $aTiO_2$-Cr_2O_3 as function of annealing temperatures did not observe much change of the valance band edge. Therefore, no doping of Cr in TiO_2 occurred in the sample after annealing.

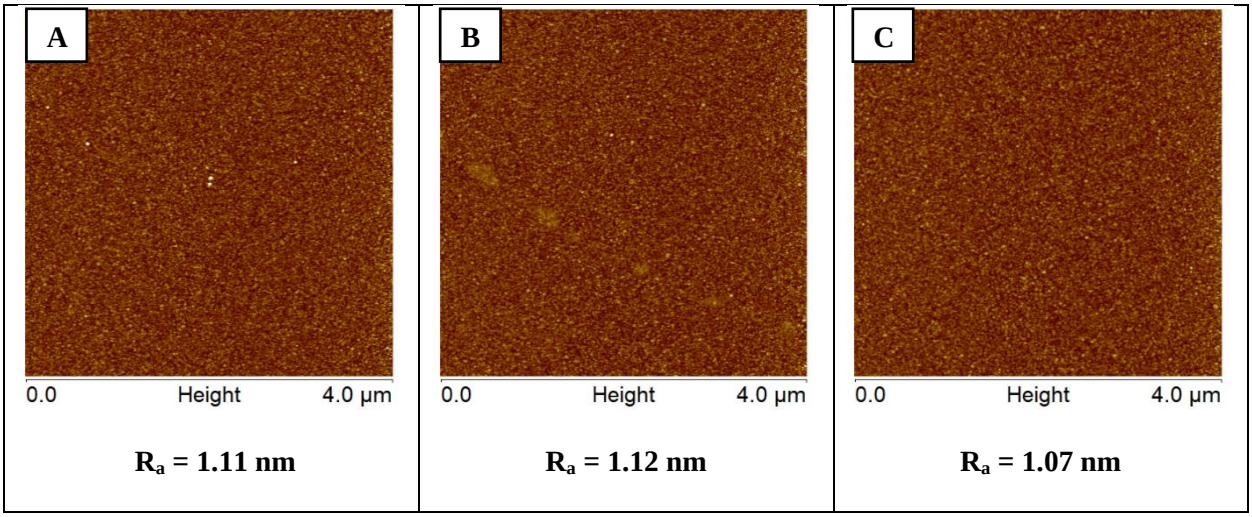

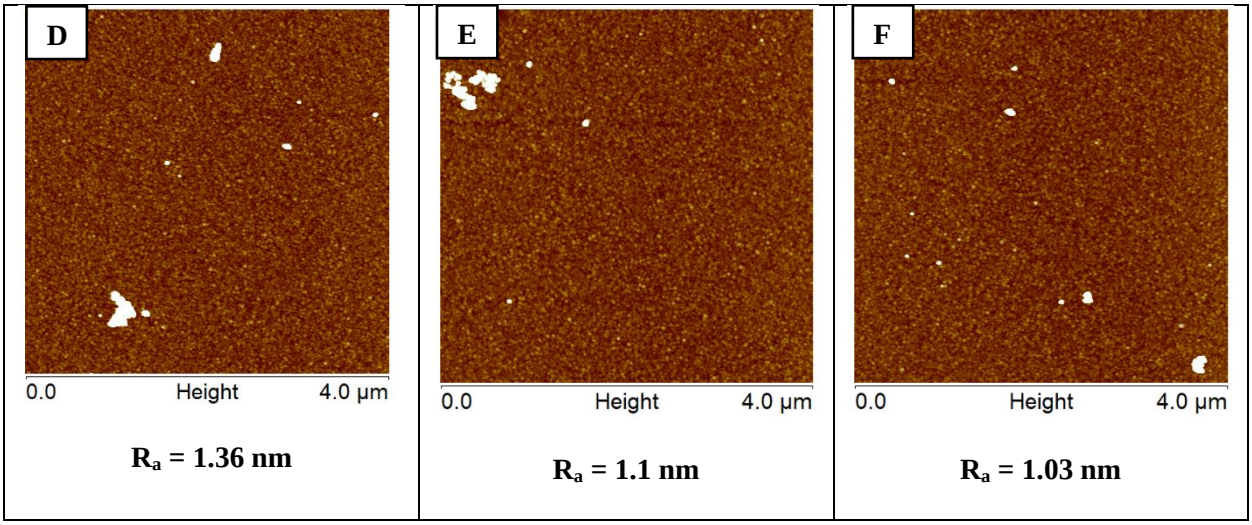

***Figure S16**: AFM images of (**A**, **B** and **C**) $aTiO_2$ and (**D**, **E** and **F**) $aTiO_2$-Cr_2O_3. (The height scale for each image is the same and is 20 nm)*

The average R_a value of the images acquired on the $aTiO_2$ surface was 1.1±0.03 nm, while the average R_a value for the $aTiO_2$ surface after the photodeposition of Cr_2O_3 layer was 1.16 ±0.17 nm. Note that the white particles increase the overall roughness and excluding these particles lead to the decrease the R_a to 0.94 ±0.04 nm.

References

1. Chambers, B. A.; Neumann, C.; Turchanin, A.; Gibson, C. T.; Andersson, G. G., The direct measurement of the electronic density of states of graphene using metastable induced electron spectroscopy. *2D Materials* **2017,** *4* (2), 025068.

2. Krischok, S.; Höfft, O.; Günster, J.; Stultz, J.; Goodman, D. W.; Kempter, V., H2O interaction with bare and Li-precovered TiO2: studies with electron spectroscopies (MIES and UPS(HeI and II)). *Surface Science* **2001,** *495* (1), 8-18.

3. Andersson, G. G.; Golovko, V. B.; Alvino, J. F.; Bennett, T.; Wrede, O.; Mejia, S. M.; Al Qahtani, H. S.; Adnan, R.; Gunby, N.; Anderson, D. P., Phosphine-stabilised Au9 Clusters Interacting with Titania and Silica Surfaces: The First Evidence for the Density of States Signature of the Support-immobilised Cluster. *The Journal of chemical physics* **2014,** *141* (1), 014702.

4. Nefedov, V. I. G., D.; Dzhurinskii, B. F.; Sergushin, N. P.; Salyn, Ya. V., The X-ray Electronic Studies of Oxides of Certain Elements. *Zh. Neorg. Khimii* **1975,** (0044-457X), 20, 2307.

5. Baikie, T.; Ahmad, Z.; Srinivasan, M.; Maignan, A.; Pramana, S. S.; White, T. J., The crystallographic and magnetic characteristics of Sr2CrO4 (K2NiF4-type) and Sr10(CrO4)6F2 (apatite-type). *Journal of Solid State Chemistry* **2007,** *180* (5), 1538-1546.

6. Torras, J.; Azambuja, D. S.; Wolf, J. M.; Alemán, C.; Armelin, E., How Organophosphonic Acid Promotes Silane Deposition onto Aluminum Surface: A Detailed Investigation on Adsorption Mechanism. *The Journal of Physical Chemistry C* **2014,** *118* (31), 17724-17736.

7. Biesinger, M. C.; Brown, C.; Mycroft, J. R.; Davidson, R. D.; McIntyre, N. S., X-ray photoelectron spectroscopy studies of chromium compounds. *Surface and Interface Analysis* **2004,** *36* (12), 1550-1563.

8. Jianjun, W.; Qunji, X., Effects of synthetic additives on the friction and wear properties of a Cr2O3 coating. *Wear* **1994,** *176* (2), 213-216.

9. Eschen, F.; Heyerhoff, M.; Morgner, H.; Vogt, J., The concentration-depth profile at the surface of a solution of tetrabutylammonium iodide in formamide, based on angle-resolved photoelectron spectroscopy. *Journal of Physics: Condensed Matter* **1995,** *7* (10), 1961-1978.

10. Wang, C.; Andersson, G. G., Measuring concentration depth profiles at liquid surfaces: Comparing angle resolved X-ray photoelectron spectroscopy and neutral impact collision scattering spectroscopy. *Surface Science* **2011,** *605* (9), 889-897.

11. Trenczek-Zajac, A.; Radecka, M.; Jasinski, M.; Michalow, K. A.; Rekas, M.; Kusior, E.; Zakrzewska, K.; Heel, A.; Graule, T.; Kowalski, K., Influence of Cr on structural and optical properties of TiO2:Cr nanopowders prepared by flame spray synthesis. *Journal of Power Sources* **2009,** *194* (1), 104-111.

12. Al Qahtani, H. S.; Metha, G. F.; Walsh, R. B.; Golovko, V. B.; Andersson, G. G.; Nakayama, T., Aggregation Behavior of Ligand-Protected Au9 Clusters on Sputtered Atomic Layer Deposition TiO2. *J. Phys. Chem. C* **2017,** *121* (20), 10781-10789.